Dynamics of photogenerated holes in surface modified α-Fe_2O_3 photoanodes for solar water splitting

Monica Barroso[a,1], Camilo A. Mesa[a], Stephanie R. Pendlebury[a], Alexander J. Cowan[a], Takashi Hisatomi[b], Kevin Sivula[b], Michael Grätzel[b], David R. Klug[a], and James R. Durrant[a,1]

[a]Department of Chemistry, Imperial College London, South Kensington Campus, London SW7 2AZ, United Kingdom; and [b]Ecole Polytechnique Fédérale de Lausanne, Laboratoire de Photonique et Interfaces, CH-1015 Lausanne, Switzerland

Edited by Thomas J. Meyer, University of North Carolina at Chapel Hill, Chapel Hill, NC, and approved June 13, 2012 (received for review December 17, 2011)

This paper addresses the origin of the decrease in the external electrical bias required for water photoelectrolysis with hematite photoanodes, observed following surface treatments of such electrodes. We consider two alternative surface modifications: a cobalt oxo/hydroxo-based (CoO_x) overlayer, reported previously to function as an efficient water oxidation electrocatalyst, and a Ga_2O_3 overlayer, reported to passivate hematite surface states. Transient absorption studies of these composite electrodes under applied bias showed that the cathodic shift of the photocurrent onset observed after each of the surface modifications is accompanied by a similar cathodic shift of the appearance of long-lived hematite photoholes, due to a retardation of electron/hole recombination. The origin of the slower electron/hole recombination is assigned primarily to enhanced electron depletion in the Fe_2O_3 for a given applied bias.

cobalt oxide | transient absorption spectroscopy | iron oxide | photoelectrochemistry

Efficient hydrogen generation from photoelectrochemical (PEC) water splitting using inorganic semiconductor photoelectrodes has been an important target of research for several decades (1–4) and considerable progress is currently being made in the development of suitable materials for this solar driven fuel synthesis (5–8). Metal oxides, including TiO_2, WO_3, $BiVO_4$, and Fe_2O_3 (1, 9–13) have continuously attracted particular interest due to their chemical stability, low cost, and optoelectronic properties. However, a major limitation for the application of those oxides in solar driven water splitting is that typically an additional electrical bias is required to simultaneously achieve the water oxidation and reduction reactions under solar irradiation. This limitation is particularly severe for materials with lower optical bandgap, such as Fe_2O_3 and $BiVO_4$ (10, 12), which on the other hand are of interest due to their enhanced absorption in the visible part of the of the solar irradiation spectrum. The development of strategies to reduce or remove this electrical bias requirement is therefore a key target of ongoing research (14, 15).

One approach, which has been shown to reduce the electrical bias required to achieve solar driven water splitting on such metal oxides, is the deposition of thin oxide overlayers on the surface of the light-absorbing photoelectrode. Surface modification with a range of catalytic and noncatalytic materials have been shown to reduce the overpotential for water photo-oxidation, including cobalt-based treatments (16), IrO_2 nanoparticles (17), and Ga_2O_3 and Al_2O_3 overlayers (18–20). Particular interest has recently focused upon in situ deposition of cobalt oxo/hydroxo-based (CoO_x) overlayers on several water oxidation photoanodes (15, 21–25), building upon reports that amorphous CoO_x layers, formed from Co(II) salts, are effective water oxidation electrocatalysts operating at moderate overpotentials (26). At present, the functional origin of the reduced requirement for electrical bias achieved by these treatments has not been unambiguously established. In some cases it has been suggested to result from catalytic function enhancing the water oxidation kinetics/reducing the overpotential required to drive water oxidation (15, 23). In other cases, the treatments have been suggested to passivate surface states, reducing the kinetics of surface recombination reactions (18, 19).

In this paper we focus upon the water photo-oxidation properties of hematite (α-Fe_2O_3) photoanodes before and after two alternative surface modifications, with CoO_x and Ga_2O_3. Surface modifications of hematite photoanodes with either of these materials have been shown to reduce by 100–200 mV the electrical bias required to enable water photo-oxidation (19, 23), but a detailed understanding of the role of these overlayers in the kinetics of the photoinduced reaction is still lacking.

Hematite is a particularly promising material for solar water splitting due to its relatively small bandgap (2.1 eV), chemical stability, widespread availability, and facile preparation by scalable methods (12). In common with most of the oxide materials of interest for photoelectrochemical water photolysis, hematite is an n-type semiconductor. This intrinsic n-type conductivity is caused by the presence of oxygen vacancies in the lattice of hematite, which are compensated by Fe^{2+} ions to guarantee electroneutrality (27, 28). Due to this intrinsic n-type doping, solar water splitting strategies with hematite have mostly employed this material as an oxidation photoelectrode, with photogenerated electrons being transported through the electrode to a back contact and then transferred to a counter electrode (typically platinum) to achieve water reduction and thus hydrogen generation (12, 29, 30). As the conduction band edge of hematite lies below the proton reduction potential, an external electrical bias is typically required in a photoelectrochemical (PEC) cell employing a hematite photoanode, to raise the energy of electrons in the cathode and achieve proton reduction. An additional role of the applied bias is to allow a partial depletion of electrons in the hematite film, thereby reducing recombination and increasing the lifetime of photogenerated holes (the minority charge carrier in these films) (31, 32). For flat photoelectrodes, this electron depletion corresponds to the formation of a surface space charge layer and the associated band bending toward the electrode surface. For nanostructured or very thin films, where the feature size may be comparable to the depletion depth (as is probably the case for the films employed herein), this band bending may be less pronounced, and the applied bias rather reduces the (dark) electron density throughout most of the film.

We have recently shown that the observation of water photo-oxidation by several oxide photoelectrodes is strongly correlated with the yield of long-lived (100 ms – seconds) photogenerated holes probed in transient optical measurements. This correlation

Author contributions: M.B. and J.R.D. designed research; M.B., C.A.M., and S.R.P. performed research; A.J.C., T.H., K.S., M.G., and D.R.K. contributed new reagents/analytic tools; M.B. analyzed data; and M.B. and J.R.D. wrote the paper.

The authors declare no conflict of interest.

This article is a PNAS Direct Submission.

[1]To whom correspondence may be addressed. E-mail: m.barroso@imperial.ac.uk or j.durrant@imperial.ac.uk.

This article contains supporting information online at www.pnas.org/lookup/suppl/doi:10.1073/pnas.1118326109/-/DCSupplemental.

was verified for a range of oxides (TiO_2, WO_3, and Fe_2O_3), for both flat and nanostructured films, and both under electrical bias control and in the presence of chemical electron scavengers (31, 33, 34). Most recently, we have demonstrated that CoO_x deposited onto a hematite film resulted in the generation of long-lived holes in the absence of applied bias, showing that this treatment resulted in a significant reduction in electron/hole recombination losses (25). In this paper, we extend these studies by reporting a transient absorption and spectroelectrochemical study of the dynamics of photogenerated charge carriers in hematite following surface treatments with CoO_x and Ga_2O_3. The photoanode systems Fe_2O_3/CoO_x and Fe_2O_3/Ga_2O_3 have been discussed recently and are representative examples of oxide overlayers with ascribed catalytic and surface passivation roles, respectively (19, 23). For that reason, these model systems were investigated under a range of applied electrical biases corresponding to different photoelectrochemical device function conditions, with the purpose of gaining new insights into how surface modifications can produce an enhancement in photoelectrode performance. On the basis of the studies presented herein, we suggest that the performance enhancement observed following the surface modifications of hematite with CoOx and Ga_2O_3 is largely a consequence of enhanced electron depletion in the photoelectrode under applied bias, resulting in a reduction of electron/hole recombination losses.

Results

Two types of mesoporous hematite films and surface overlayer treatments were considered in this study. The first type, silicon-doped α-Fe_2O_3 grown by an atmospheric pressure vapor deposition (APCVD) technique (hereafter designated APCVD hematite), exhibits a cauliflower-like nanostructure with feature sizes in the order of 5–10 nm and has recently demonstrated the highest solar water oxidation photocurrents for an oxide-based photoanodes tested under standard conditions (17). A thin layer of amorphous CoO_x was electrodeposited on the surface of these photoanodes from a Co(II) solution in aqueous phosphate buffer. For the second type of electrodes, ultrathin hematite films (approximately 20 nm) were prepared by ultrasonic spray pyrolysis (USP) (hereafter designated USP hematite) (35). These electrodes were subsequently modified with a Ga_2O_3 overlayer by chemical bath deposition (CBD) (19). The choice of USP films instead of the better performing APCVD for the investigation of the role of Ga_2O_3 is due to the detrimental effect that CBD conditions have on the quality of films prepared by APCVD (19). Ultrathin USP films were preferred in order to enhance the effect of Ga_2O_3 modification.

Both the CoO_x and Ga_2O_3 treatments resulted in cathodic shifts of the water oxidation photocurrent onset by more than 100 mV (Fig. 1), consistent with previous observations (19, 23). We note that, in contrast, a cathodic shift of the dark current was observed with the Co-Pi treatment while an anodic shift was observed with the Ga_2O_3 modification, consistent with the corresponding water oxidation electrocatalytic activities (19, 26). Photocurrent measurements under chopped illumination (Fig. S1) show a cathodic shift of the transient charging currents at modest applied bias for both treatments, assigned to the passivation of surface trapping sites by the oxide overlayers (19, 20, 23). In addition we note that neither surface modification resulted in a significant shift in the onset of photocurrent transients, in agreement with previous observations (22, 24), suggesting that the flat band potential of the photoelectrode remains unchanged. We have reported qualitatively similar photocurrent onset shifts with CoO_x treatment of USP hematite photoanodes (25) and have observed similar trends upon Co^{2+} adsorption on APCVD and ultrathin USP hematite used in this study. Furthermore, surface adsorption of Co^{2+} on Ga_2O_3 modified photoanodes produced an additional cathodic shift of the photocurrent onset, confirming the cumulative

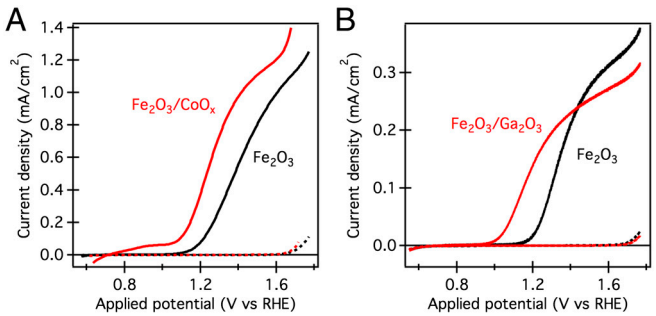

Fig. 1. Photocurrent-potential curves of mesoporous hematite photoanodes before and after surface modification. (*A*) APCVD hematite without (black) and with (red) CoO_x overlayer; (*B*) ultrathin USP hematite without (black) and with (red) Ga_2O_3 overlayer. Measurements in 0.1 M NaOH (pH 12.6), at 10 mV s^{-1}, in dark (dashed lines) and illuminated with simulated sunlight (approximately 1 Sun, AM 1.5G) through the electrolyte-electrode (EE) interface.

enhancement of photoelectrochemical performance caused by the two modifications (Fig. S2) (19).

We turn now to consideration of the impact of the two surface modifications upon the kinetics of photogenerated charge carriers in hematite. Fig. 2 shows transient absorption data observed following low intensity pulsed excitation at 355 nm in the absence of an external bias. The data monitors the photoinduced absorption at 700 nm, representative of the broad photoinduced absorption observed between 550 and 900 nm, previously assigned to photogenerated Fe_2O_3 holes based on the faster decay rate of these transients in the presence of methanol (31). The decay kinetics of these photoholes in APCVD and USP hematite are very similar. It is apparent that the CoO_x treatment results in a very significant (three orders of magnitude) increase in the lifetime of photogenerated holes, as we have reported previously (25). A smaller increase in hole lifetime is also observed when hematite is treated by surface adsorption of Co^{2+} ions (Fig. S3). In contrast, the Ga_2O_3 treatment does not significantly increase the hole lifetime in the absence of applied bias.

Fig. 3 shows the corresponding dynamics of photogenerated hole absorption at 700 nm before and after surface modification of hematite, as a function of applied bias. In both cases, for the untreated electrodes (Fig. 3 *A* and *C*) it is apparent that at sufficiently anodic bias the hole decay dynamics become biphasic. The fast phase (lifetime up to approximately 10 ms) is assigned to electron/hole recombination (36). The lifetime of this phase is increased under high anodic bias conditions, assigned, as pre-

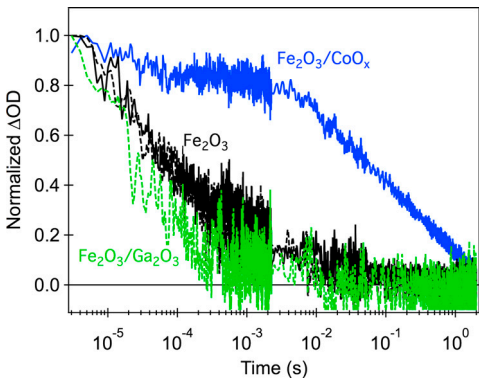

Fig. 2. Normalized transient absorption decays of hematite photoholes probed at 700 nm and obtained with front-side low-intensity UV illumination (355 nm, 0.2 mJ/cm^2, 0.33 Hz) of isolated hematite photoanodes, immersed in 0.1 M NaOH aqueous solution. Bare Fe_2O_3 films are shown in black, Fe_2O_3/CoO_x is shown in blue, and Fe_2O_3/Ga_2O_3 is shown in green. Decay traces corresponding to APCVD hematite are depicted with full lines and to USP hematite with dashed lines.

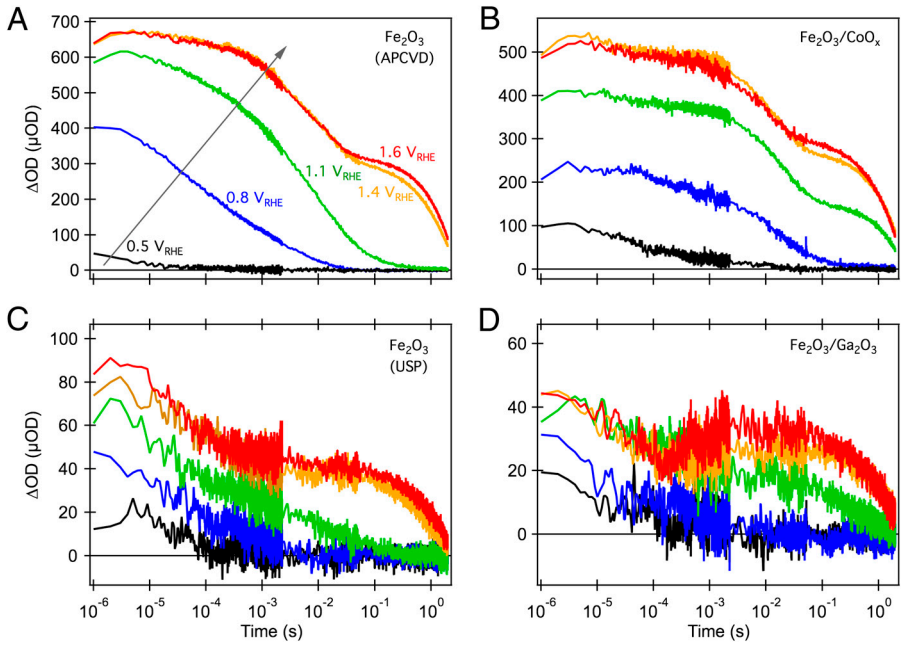

Fig. 3. Electrical bias dependence of transient absorption decays probed at 700 nm following excitation at 355 nm of bare (*A* and *C*) and treated (*B* and *D*) Fe_2O_3 photoanodes. The right column shows the effect of surface modification of the photoanodes with CoO_x (*Top*, *B*) and Ga_2O_3 (*Bottom*, *D*). The color code for the applied potentials is shown in Fig. 3*A*. (V_{RHE} represents the applied potential relative to the reversible hydrogen electrode, RHE).

viously, to slower electron/hole recombination due to enhanced electron depletion in the photoelectrode at such bias conditions (36). We note here that faster recombination phases are also likely (13, 37, 38) although not resolved in the studies reported herein. In addition, a slow (approximately 2-s) decay phase is observed, assigned to long-lived holes, whose amplitude increases with increasingly anodic bias.

We have previously shown that the amplitude of the long-lived hole signal correlates with photocurrent density for both TiO_2 and hematite photoelectrodes (33, 36). Qualitatively similar biphasic decays were observed for the nanostructured APCVD hematite before and after CoO_x treatment (Fig. 3 *A* and *B*) and for the ultrathin USP hematite without and with Ga_2O_3 overlayer (Fig. 3 *C* and *D*). However, quantitative analysis shows a striking shift in the bias dependence of the amplitude of the long-lived hole signal—with, for example, the data at 1.1 V_{RHE} applied bias in Fig. 3 showing negligible long-lived holes in the absence of surface modification but a clear long-lived hole signal in the presence of CoO_x or Ga_2O_3.

Fig. 4 plots the amplitude of the long-lived (2-s lifetime) hole signal as a function of applied bias for the electrodes studied herein. It is apparent that the CoO_x and Ga_2O_3 treatments result, respectively, in an approximately 150 ± 50 mV and 100 ± 25 mV cathodic shift of the appearance of these long-lived transients. This cathodic shift of long-lived hole generation correlates well with the cathodic shift of photocurrent generation observed above (Fig. 1) (33, 36). It is striking that the two surface treatments result in very different effects on the charge carrier dynamics in the absence of applied bias but rather similar effects under applied bias. The origin of this behavior will be discussed below.

We turn now to other signatures of the influence of surface treatment upon the photoelectrode activity as a function of applied bias, focusing in particular upon the CoO_x treatment. Fig. 5 shows spectroelectrochemical data for a hematite photoanode without and with CoO_x overlayer, plotting the change in UV/visible absorption as a function of increasingly anodic applied bias. For the untreated film, the anodic bias results in the appearance of a well-defined positive absorption band peaking at 580 nm. This positive absorption band is assigned to localized intra-bandgap states. Its observation for applied potentials only mildly positive of the Fe_2O_3 conduction band suggests that these states lie a few hundred millivolts below the conduction band. The observation of a positive absorption with increasing positive applied bias indicates that it derives from the oxidized form of this intraband redox state. The nature and function of these states will be discussed further below. For the CoO_x treated film, the appearance of this 580-nm absorption band is superimposed upon a broader positive absorption, assigned to the oxidation of cobalt II or III ions present in the CoO_x layer (39). Of particular interest to this paper is the bias dependence of the appearance of the 580-nm absorption feature, as plotted in Fig. 5*C*. It is apparent that CoO_x treatment results in an approximately 100-mV cathodic shift in the bias dependence of this feature, analogous to the cathodic shifts of the photocurrent and long-lived hole signals reported above.

Finally we consider the full transient absorption spectral response of APCVD Fe_2O_3 with and without CoO_x overlayer as a function of applied bias. Fig. 6 summarizes the transient absorption features observed between 500 and 900 nm for bare and CoO_x-treated films at four different applied biases. The color coding in the figure corresponds to spectra measured at different time delays, ranging from 1 μs (gray) to 2 s (red). It is apparent

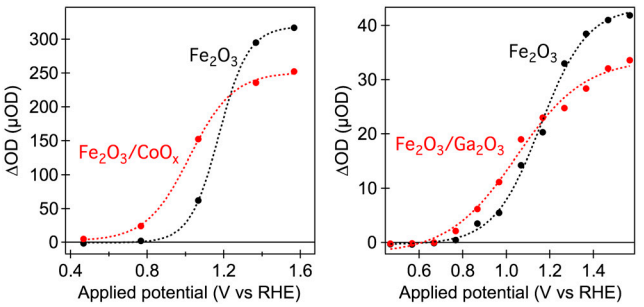

Fig. 4. Amplitude of the 700-nm transient absorption measured at 50 ms after laser excitation, as a function of applied bias, for APCVD hematite before and after surface modification with CoO_x (*Left*) and for ultrathin USP hematite before and after surface modification with Ga_2O_3 (*Right*). The dotted lines are intended to guide the eye and are not fits to a specific model.

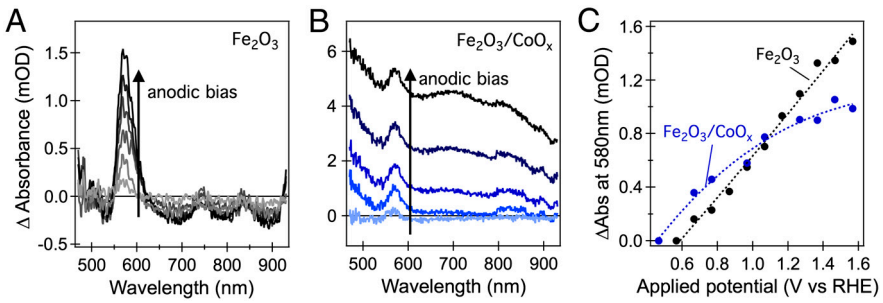

Fig. 5. Spectroelectrochemistry of hematite photoanodes. (*A*) Difference absorption spectra of a bare hematite photoanode measured at various potential biases in the range 0.7 V–1.6 V relative to 0.6 V vs RHE; (*B*) difference absorption spectra of a Fe_2O_3/CoO_x photoanode measured at various potential biases in the range 0.6 V–1.6 V relative to 0.5 vs RHE. (*C*) Absorption difference measured at 580 nm as a function of applied bias for the bare hematite photoanode (black) and the Fe_2O_3/CoO_x photoanode (blue). The dotted lines are intended to guide the eye and are not fits to a specific model.

that the application of high anodic bias results in the generation of a broad, long-lived absorption with a maximum at approximately 650 nm, apparent from the spectra at time delays of 100 ms–2 s under 1.6 V_{RHE} (Fig. 6*D*), and evidenced also in Fig. 6*E*. The spectrum of this broad signal is independent of CoO_x treatment and distinct from the absorption increase assigned to cobalt oxidation observed in the spectroelectrochemical data above. It is therefore assigned, as discussed previously (31, 36), to hematite holes. In contrast to our previous studies in the absence of applied bias (25), with bias control no long-lived bleaching signal is observed. This bleach was assigned previously to bleaching of cobalt oxide ground state absorption.

The broad, long-lived signal (>100 ms) assigned to Fe_2O_3 holes is apparent at a bias of 1.1 V_{RHE} in Fe_2O_3/CoO_x but is not observed at this voltage in the untreated hematite photoelectrode (Fig. 6*C*), consistent with the cathodic shift of appearance of this long-lived hole signal discussed above. The spectral signature of long-lived holes in hematite is shown in Fig. 6*E*, measured 1 s after laser excitation under various applied bias, in Fe_2O_3 and Fe_2O_3/CoO_x electrodes. It is apparent that CoO_x treatment causes a cathodic shift in the appearance of this long-lived signal but does not significantly change its shape, confirming that for both the treated and untreated films, this long-lived signal derives from hematite holes. Similarly the decay dynamics of this long-lived signal (Fig. 3 *A* and *B*), and indeed the full spectral data observed under strong anodic bias (Fig. 6*D*), are all independent of CoO_x treatment. We therefore conclude that while CoO_x does change the bias dependence of the yield of hematite holes, it does not change the lifetime of the long-lived transients.

Superimposed upon the broad, long-lived, hematite hole absorption, more complex behavior is observed at earlier times (up to approximately 100 ms) between 500 and 600 nm. In particular, a relatively intense, narrow absorption feature is observed peaking at approximately 580 nm as well as a smaller feature peaking at approximately 540 nm for intermediate biases. Both of these features have largely disappeared by 100 ms in the potential range investigated. Under cathodic bias in the absence of CoO_x, the 580 nm band corresponds to a positive transient absorption increase. Both CoO_x treatment and more positive applied bias result in a progressive inversion of this feature, leading to a large absorption bleach peaking at 580 nm, whose magnitude increases with increasingly positive bias.

The 580 nm absorption feature observed in our transient absorption studies (either in isolated electrodes or those under external bias control) is assigned to the same intra-bandgap state absorption observed in our spectroelectrochemical data discussed above and shown in Fig. 5. Following that discussion, the positive transient feature observed at 580 nm for cathodic bias in the absence of CoO_x is assigned to oxidation of pre-reduced intraband states—corresponding, in this case, to hole trapping. This positive feature was also observed in absence of applied bias and was most pronounced in undoped Fe_2O_3 films (25, 31). Under anodic bias, these intraband states become increasingly pre-oxidized. As such, these states function increasingly as electron traps, becoming transiently reduced following the laser pulse and generating the observed transient absorption bleach. We note that this 580 nm transient absorption feature decays completely in approximatley 10 ms, two orders of magnitude faster than the decay of the long-lived holes assigned to water oxidation.

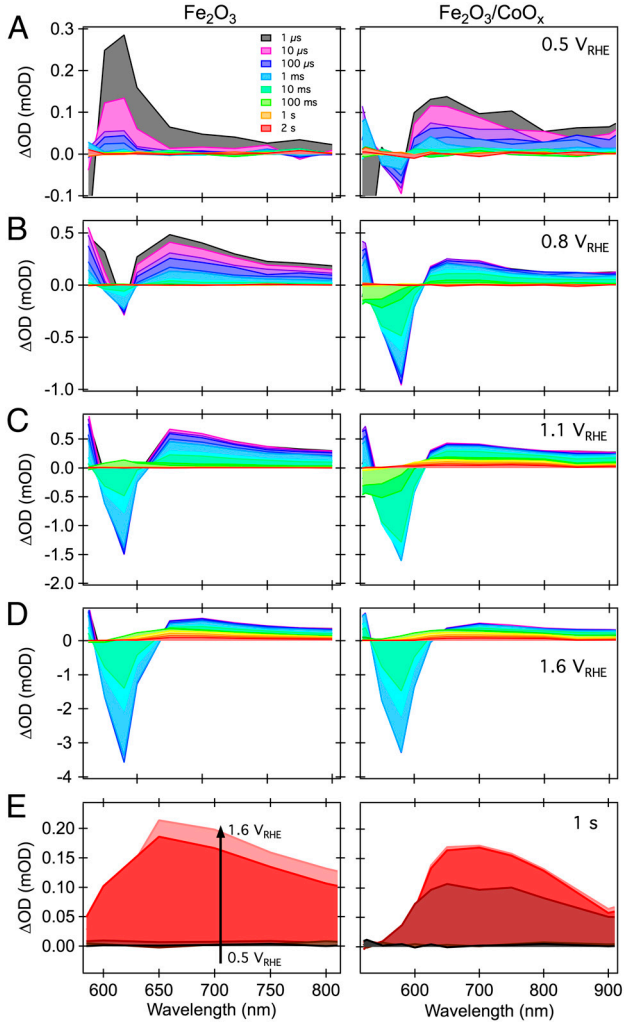

Fig. 6. Time evolution of the transient absorption spectra of Fe_2O_3 (*Left*) and Fe_2O_3/CoO_x (*Right*) photoelectrodes, under external applied bias: (*A*) 0.5 V_{RHE}, (*B*) 0.8 V_{RHE}, (*C*) 1.1 V_{RHE}, and (*D*) 1.6 V_{RHE}, as indicated. (*E*) Bias dependence of the appearance of long-lived hematite photoholes, probed at 1 s after laser excitation.

Discussion

Water splitting is a kinetically and thermodynamically difficult process. The concerted oxidation of two molecules of water to give one molecule of oxygen requires four holes (or "oxidizing equivalents"), and as such is strongly dependent upon the presence of suitably catalytic sites to enable this multi-electron chemistry (40). Alternatively, photogenerated holes can oxidize water via a series of sequential one-hole oxidation reactions, which are thermodynamically less favorable but do not require the accumulation of multiple oxidizing equivalents at a catalytic site. Our previous study of the activation energy for the reaction of photogenerated hematite holes with water suggested that these charge carriers primarily oxidize water via a series of one-hole oxidation steps (34). We obtained further support for this conclusion from our observation that the kinetics of this oxidation reaction, and the overall photocurrent generation efficiency, were independent of light intensity and therefore hole density (36). This sequential reaction pathway is most probably enabled by the highly oxidizing nature of hematite valence band holes and suggests that the efficiency of water oxidation by hematite photoelectrodes may not be strongly dependent upon the introduction of catalytic multi-electron water oxidation sites on its surface (34). We note that this lack of requirement for catalytic sites results from the highly oxidising nature of hematite photoholes; for photoelectrodes with less oxidizing valence bands, the introduction of catalytic sites can be expected to be critical to achieve efficient water photo-oxidation.

From our previous work, it appears that a key requirement for water photo-oxidation by hematite is that light absorption must generate photoholes with sufficient lifetime to be able to oxidize water (32). Our transient kinetic studies also suggest that the lifetime required for water oxidation by hematite photoholes is on the order of 1 s, a conclusion supported by recent frequency domain photoelectrochemical analyses (18, 32, 41). In particular, we observe here a close correlation between the bias dependence of the appearance of the long-lived photohole transient signal and the bias requirement for the observation of anodic photocurrents, providing further confirmation of requirement of long-lived holes to enable water oxidation.

The observation of a cathodic shift in the bias dependence of water oxidation photocurrents upon the deposition of CoO_x on hematite, as well as with other cobalt treatments (most likely also leading to the formation of related CoO_x layers), was initially assigned, at least in part, to catalytic function of the cobalt-based layer in accelerating water oxidation (20). In the studies we report herein, and previously (2, 25), we find no evidence to support this conclusion. Our spectroelectrochemical studies show evidence of cobalt oxidation under positive applied bias for the CoO_x-treated film. However, our transient studies indicate that the lifetime of long-lived photogenerated Fe_2O_3 holes is independent of CoO_x and in operating conditions (studies under bias control) show no evidence for the transfer of photogenerated hematite holes to the cobalt-based overlayer. A similar conclusion was recently reported for hematite films with Co^{2+} ions adsorbed at the hematite surface (42). As such, while it has been widely reported that CoO_x deposited on conducting substrates such as ITO is an effective electrocatalyst, reducing the overpotential required for electrochemical water oxidation (26), the cathodic shifts of photocurrent generation by hematite photoelectrodes induced by cobalt-based treatments do not appear to result primarily from this catalytic function. It is therefore necessary to consider alternative explanations for the enhanced photoelectrochemical performance.

There is extensive previous literature on the presence of intra-bandgap bulk traps and surface states on hematite and their potential role as recombination centers (30, 43, 44). Several recent studies have suggested that the cathodic shift of photocurrent generation by CoO_x and other treatments such as with Ga_2O_3 or Al_2O_3 overlayers may result from passivation of surface recombination sites, thereby partially suppressing surface recombination (19, 20, 22). We note that there is some ambiguity in the nature of these "surface states" and particularly whether this term refers only to states at the molecular scale electrode–electrolyte interface or also includes a finite region extending into the semiconductor (e.g., the space charge layer). In this regard, it is of particular note that the Ga_2O_3 treatment reported herein did not result in a significant retardation of electron/hole recombination in the absence of applied bias—suggesting that while this treatment may well passivate surface states, this passivation alone is not sufficient to significantly influence electron/hole recombination.

A related explanation for the photocurrent onset shifts observed following both CoO_x and Ga_2O_3 treatments is that they may influence the electron density in the Fe_2O_3 photoelectrode, thereby retarding electron/hole recombination. We have previously attributed the increase in hole lifetime in the absence of applied bias following surface modification with CoO_x to such a decrease in electron density (25). This effect was assigned to the oxidizing nature of the surface modification that resulted in the development of a partial electron depletion of the Fe_2O_3, indicative of the formation of an Fe_2O_3/CoO_x heterojunction. This assignment is consistent with the lack of any increase in hole lifetime following Ga_2O_3 treatment, which involves the deposition of a redox inactive oxide layer and therefore would not be expected to result in electron depletion in the hematite film.

Enhanced electron depletion of the Fe_2O_3 can also be invoked to explain the behavior of photoanodes under operating conditions (i.e., under external bias control), shown in Fig. 3. In the limit of strong cathodic bias, both the CoO_x- and Ga_2O_3-treated films exhibit rapid hole decay dynamics, indicative of rapid electron/hole recombination induced by the high electron densities present in the films at these potentials. As the bias is shifted increasingly anodic, electron/hole recombination is retarded, leading to the formation of long-lived holes. The cathodic shift of the appearance of long-lived holes observed following CoO_x and Ga_2O_3 treatments can, thus, be attributed to a cathodic shift in the development of electron depletion in the Fe_2O_3. Further support for such a shift can be obtained from our spectroelectrochemical data for the 580-nm absorption feature assigned to localized intra-band states of the Fe_2O_3. The magnitude of this signal can be used as an indicator of the redox occupancy of these states and thus of the photoanode's Fermi level relative to the flatband potential. In this regard, it is striking that the spectroelectrochemical data shows a cathodic shift of the 580-nm absorption signal in the presence of CoO_x (Fig. 5*C*), indicating an increased electron depletion of the film following this surface modification.

It follows from the above arguments that the most likely origin of the cathodic shifts in photocurrent onset observed following both CoO_x and Ga_2O_3 treatments is a reduced electron density in the hematite, reducing electron/hole recombination and increasing the yield of long-lived holes at the electrode surface. Such increased electron depletion following the CoO_x and Ga_2O_3 treatments most likely results from surface state passivation, in agreement with several previous reports (19, 20, 22). The presence of high densities of surface states causes Fermi level pinning at the energies corresponding to such states and a consequent decrease in the space charge layer width. Passivation of these states will enhance electron depletion within the film for a given bias, consistent with the results reported herein. We note that the enhanced electron depletion observed following CoO_x treatment is also likely to be associated, at least in part, with the redox active nature of the cobalt oxide layer, as we have discussed previously (in the absence of applied bias, this is most probably the dominant cause of the slower electron/hole recombination observed following CoO_x treatment) (25). We conclude

that these surface treatments result in a cathodic shift of the photocurrent, not primarily by removing surface recombination centers or enhancing the kinetics of water photo-oxidation but rather by enhancing the spatial extent or magnitude of the space charge/electron depletion layer. As such, these results emphasize that one materials design strategy to enhance performance of water oxidation photoanodes, particularly those whose efficiency is limited by electron-hole recombination losses, is to target specifically the enhancement of electron depletion within the photoelectrode while still ensuring sufficient conductivity through the film to allow electron extraction without large ohmic losses. Such strategies could include not only surface modification but also new architectures to enable efficient electron conduction without the requirement for chemical doping, such as core/shell and related approaches (13, 14).

Materials and Methods

A detailed description of the materials and methods used in this work is given in *SI Text*.

All the applied potentials reported in this work are relative to the reversible hydrogen electrode (RHE) and are obtained from those relative to the Ag/AgCl/0.3 M KCl (SSC) reference electrode using the Nernst equation, $E_{RHE} = E^0{}_{SSC} + E_{SSC} + 0.059$ pH, where $E^0{}_{SSC}$ is the standard potential of the SSC reference (0.21 V_{RHE} at 25 °C) and E_{SSC} is the potential measured versus the SSC.

ACKNOWLEDGMENTS. We thank Dr. Christopher Barnett for equipment development and maintenance, SocMan Ho Kimura for lab support, and Dr. Piers Barnes for helpful discussions. Financial support from the Engineering and Physical Sciences Resarch Council, the European Research Council (Project Intersolar), the Swiss Federal Office of Energy (Project 102326, PECHouse), and the European Commission's Framework Project 7 (NanoPEC, Project 227179) are gratefully acknowledged.

1. Fujishima A, Honda K (1972) Electrochemical photolysis of water at a semiconductor electrode. *Nature* 238:37–38.
2. Bard AJ, Fox MA (1995) Artificial photosynthesis: Solar splitting of water to hydrogen and oxygen. *Acc Chem Res* 28:141–145.
3. Gratzel M (2001) Photoelectrochemical cells. *Nature* 414:338–344.
4. Walter MG, et al. (2010) Solar water splitting cells. *Chem Rev* 110:6446–6473.
5. Osterloh FE (2008) Inorganic materials as catalysts for photochemical splitting of water. *Chem Mater* 20:35–54.
6. Kudo A, Miseki Y (2009) Heterogeneous photocatalyst materials for water splitting. *Chem Soc Rev* 38:253–278.
7. Maeda K (2011) Photocatalytic water splitting using semiconductor particles: History and recent developments. *J Photochem Photobiol C* 12:237–268.
8. Bak T, Nowotny J, Rekas M, Sorrell CC (2002) Photo-electrochemical hydrogen generation from water using solar energy. Materials-related aspects. *Int J Hydrogen Energy* 27:991–1022.
9. Santato C, Odziemkowski M, Ulmann M, Augustynski J (2001) Crystallographically oriented mesoporous WO3 films: Synthesis, characterization, and applications. (Translated from English). *J Am Chem Soc* 123:10639–10649 (in English).
10. Berglund SP, Flaherty DW, Hahn NT, Bard AJ, Mullins CB (2011) Photoelectrochemical oxidation of water using nanostructured BiVO4 films. (Translated from English). *J Phys Chem C* 115:3794–3802 (in English).
11. Iwase A, Kudo A (2010) Photoelectrochemical water splitting using visible-light-responsive BiVO4 fine particles prepared in an aqueous acetic acid solution. (Translated from English). *J Mater Chem* 20:7536–7542 (in English).
12. Sivula K, Le Formal F, Grätzel M (2011) Solar water splitting: Progress using hematite (α-Fe_2O_3) photoelectrodes. *Chem Sus Chem* 4:432–449.
13. Kronawitter CX, et al. (2011) A perspective on solar-driven water splitting with all-oxide hetero-nanostructures. *Energy Environ Sci* 4:3889–3899.
14. Lin Y, Zhou S, Sheehan SW, Wang D (2011) Nanonet-based hematite heteronanostructures for efficient solar water splitting. *J Am Chem Soc* 133:2398–2401.
15. Zhong DK, Choi S, Gamelin DR (2011) Near-complete suppression of surface recombination in solar photoelectrolysis by "Co-Pi" catalyst-modified W:BiVO4. *J Am Chem Soc* 133:18370–18377.
16. Kay A, Cesar I, Gratzel M (2006) New benchmark for water photooxidation by nanostructured α-Fe_2O_3 films. *J Am Chem Soc* 128:15714–15721.
17. Tilley SD, Cornuz M, Sivula K, Grätzel M (2010) Light-induced water splitting with hematite: Improved nanostructure and iridium oxide catalysis. *Angew Chem Intl Ed Engl* 49:6405–6408.
18. Le Formal F, et al. (2011) Passivating surface states on water splitting hematite photoanodes with alumina overlayers. (Translated from English). *Chem Sci* 2:737–743 (in English).
19. Hisatomi T, et al. (2011) Cathodic shift in onset potential of solar oxygen evolution on hematite by 13-group oxide overlayers. *Energy Environ Sci* 4:2512–2515.
20. Spray RL, McDonald KJ, Choi K-S (2011) Enhancing photoresponse of nanoparticulate α-Fe_2O_3 electrodes by surface composition tuning. *J Phys Chem C* 115:3497–3506.
21. Steinmiller EMP, Choi KS (2009) Photochemical deposition of cobalt-based oxygen evolving catalyst on a semiconductor photoanode for solar oxygen production. *Proc Natl Acad Sci USA* 106:20633–20636.
22. Seabold JA, Choi K-S (2011) Effect of a cobalt-based oxygen evolution catalyst on the stability and the selectivity of photo-oxidation reactions of a WO3 photoanode. *Chem Mater* 23:1105–1112.
23. Zhong DK, Cornuz M, Sivula K, Gratzel M, Gamelin DR (2011) Photo-assisted electrodeposition of cobalt-phosphate (Co-Pi) catalyst on hematite photoanodes for solar water oxidation. *Energy Environ Sci* 4:1759–1764.
24. McDonald KJ, Choi K-S (2011) Photodeposition of co-based oxygen evolution catalysts on α-Fe_2O_3 photoanodes. *Chem Mater* 23:1686–1693.
25. Barroso M, et al. (2011) The role of cobalt phosphate in enhancing the photocatalytic activity of α-Fe_2O_3 toward water oxidation. (Translated from English). *J Am Chem Soc* 133:14868–14871 (in English).
26. Kanan MW, Surendranath Y, Nocera DG (2009) Cobalt-phosphate oxygen-evolving compound. *Chem Soc Rev* 38:109–114.
27. Gardner RFG, Tanner DW, Sweerr F (1963) Electrical properties of alpha ferric oxide. 2. Ferric oxide of high purity. *J Phys Chem Solids* 24:1183–1186.
28. Ahmed SM, Leduc J, Haller SF (1988) Photoelectrochemical and impedance characteristics of specular hematite. 1. Photoelectrochemical, parallel conductance, and trap rate studies. *J Phys Chem* 92:6655–6660.
29. Kennedy JH, Frese KW (1978) Photooxidation of Water at α-Fe_2O_3 Electrodes. *J Electrochem Soc* 125:709–714.
30. Dare-Edwards MP, Goodenough JB, Hamnett A, Trevellick PR (1983) Electrochemistry and photoelectrochemistry of iron(III) oxide. *J Chem Soc Faraday Trans* 79:2027–2041.
31. Pendlebury SR, et al. (2011) Dynamics of photogenerated holes in nanocrystalline α-Fe_2O_3 electrodes for water oxidation probed by transient absorption spectroscopy. *Chem Comm* 47:716–718.
32. Wijayantha KGU, Saremi-Yarahmadi S, Peter LM (2011) Kinetics of oxygen evolution at α-Fe_2O_3 photoanodes: A study by photoelectrochemical impedance spectroscopy. *Phys Chem Chem Phys* 13:5264–5270.
33. Cowan AJ, Tang JW, Leng WH, Durrant JR, Klug DR (2010) Water splitting by nanocrystalline TiO2 in a complete photoelectrochemical cell exhibits efficiencies limited by charge recombination. *J Phys Chem C* 114:4208–4214.
34. Pesci FM, Cowan AJ, Alexander BD, Durrant JR, Klug DR (2011) Charge carrier dynamics on mesoporous WO3 during water splitting. *J Phys Chem Lett* 2:1900–1903.
35. Le Formal F, Gratzel M, Sivula K (2010) Controlling photoactivity in ultrathin hematite films for solar water-splitting. *Adv Funct Mater* 20:1099–1107.
36. Pendlebury SR, et al. (2012) Correlating long-lived photogenerated hole populations with photocurrent densities in hematite water oxidation photoanodes. *Energy Environ Sci* 5:6304–6312.
37. Ling Y, Wang G, Wheeler DA, Zhang JZ, Li Y (2011) Sn-doped hematite nanostructures for photoelectrochemical water splitting. *Nano Lett* 11:2119–2125.
38. Cherepy NJ, Liston DB, Lovejoy JA, Deng HM, Zhang JZ (1998) Ultrafast studies of photoexcited electron dynamics in gamma- and alpha-Fe_2O_3 semiconductor nanoparticles. *J Phys Chem B* 102:770–776.
39. Dafonseca CNP, Depaoli MA, Gorenstein A (1994) Electrochromism in cobalt oxide thin-films grown by anodic electroprecipitation. *Sol Energy Mater Sol Cells* 33:73–81.
40. Dau H, et al. (2010) The mechanism of water oxidation: From electrolysis via homogeneous to biological catalysis. *ChemCatChem* 2:724–761.
41. Klahr B, Gimenez S, Fabregat-Santiago F, Bisquert J, Hamann TW (2012) Electrochemical and photoelectrochemical investigation of water oxidation with hematite electrodes. *Energy Environ Sci* 5:7626–7636.
42. Peter LM, Wijayantha KGU, Tahir AA (2012) Kinetics of light-driven oxygen evolution at α-Fe_2O_3 electrodes. *Faraday Discuss* 155:309–322.
43. Sanchez C, Sieber KD, Somorjai GA (1988) The photoelectrochemistry of niobium doped α-Fe_2O_3. *J Electroanal Chem* 252:269–290.
44. Horowitz G (1983) Capacitance voltage measurements and flat-band potential determination on Zr-doped alpha-Fe_2O_3 single-crystal electrodes. *J Electroanal Chem* 159:421–436.